The glass transition behaviors of low-density amorphous ice films with different thicknesses

3 AUTHORS, INCLUDING:

Cheng He
Xi'an Jiaotong University

11 PUBLICATIONS   23 CITATIONS

The glass transition behaviors of low-density amorphous ice films with different thicknesses

Cheng He,[1,a)] Wenxue Zhang,[2] and Yu Li[1]

[1]*State Key Laboratory for Mechanical Behavior of Materials, School of Materials Science and Engineering, Xi'an Jiaotong University, Xi'an 710049, China*
[2]*School of Materials Science and Engineering, Chang'an University, Xi'an 710064, Shaanxi, China*

The glass transition behaviors of amorphous ice with different thicknesses are studied by determining the heat capacity of low-density amorphous ice without crystallization using first principle molecular dynamics (FP-MD) and classical MD methods. The behaviors are also studied by analyzing hydrogen-bond network, the radial distribution functions, and relationship between hydrogen bond and electronic structures. It is found that the glass transition temperature (T_g) in the range of $90 \text{ K} < T < 100 \text{ K}$ for 4 nm amorphous ice film by FP-MD method, and $120 \text{ K} < T_g < 130 \text{ K}$ for 8 nm amorphous ice film by MD method. Meanwhile, T_g decreases with the decreasing thickness of amorphous ice film, which is also validated by the theoretical model. © *2010 American Institute of Physics*. [doi:10.1063/1.3507900]

I. INTRODUCTION

At temperatures and pressures lower than those of Earth's biosphere, water freezes not in a crystalline phase, but in an amorphous one. There has been a great deal of debate to argue whether different structures represent frozen versions of different liquid polymorphs of water with an associated phase transition.[1] These same amorphous ices are of interest to astronomers[2] as dust grains in interstellar space are typically covered with an icy film formed at very low temperature of the interstellar medium (3–90 K). It has been estimated that most of the ice in the universe is to be found.[3] Much astrochemistry is presumed to take place on these icy surfaces, and larger icy bodies such as comets and Kuiper-belt objects are supposed to form due to its accretion. With the science and technology development, attention has been paid to the nanoscale interstellar dust grains. As the thickness of the amorphous ice film decreases into the nanoscale regime, the surface/volume ratio increases, this decreases the atomic cohesive energy of the film due to the presence of the coordination imperfection at the surface and the amount of average hydrogen of amorphous ice. Hence, the behaviors of these nanoscaled ice films are apparently different from bulk case especially for the glass transition temperature.

However, even in the bulk system, the nature of the glass transition of water is considered as a major intellectual challenge.[4,5] In this case, the low-density amorphous ice (LDA) can be achieved by cooling the water rapidly at a rate of 10^6 K s^{-1} or be acquired by annealing the high-density amorphous ice (HDA).[6] Meanwhile, the amorphous phase can be transformed to liquid water by heating at ambient pressure. The corresponding transition temperature is called as glass transition temperature T_g.[7] The conversion between different glass structures and the relation between the liquid and the glass phases are still under active debate. A particular relevant aspect of this debate concerns the identification of the glass transition temperature at ambient pressure and the magnitude of the associated jump of the heat capacity. Extrapolation of T_g in binary aqueous solutions, in the limit of vanishing solute concentration, provides the estimate $T_g \approx 136 \text{ K}$.[8] This T_g value[9,10] has been recently debated.[4,11,12] It has been suggested[12] that the small peak measured in Ref. 8 is a typical prepeak of annealed hyperquenched samples preceding the true glass transition located at $T_g \approx 165 \text{ K}$. Assigning $T_g \approx 165 \text{ K}$ would explain some of the puzzles related to the glass transition of amorphous ice.[9,11–13] However, this T_g is difficult to measure experimentally because water crystallizes at ~150 K. In our previous study,[14] T_g of the bulk sample is determined to be about 171 K using the heating rate of $q = 3 \times 10^{11} \text{ K s}^{-1}$. But, under the standard heating condition, i.e., at $q = 0.167 \text{ K s}^{-1}$,[15] the standard T_g value is found to be 164 K.[14] These support the estimated transition temperature of 165K.[12]

Based on the above literature results,[15] the glass transition of bulk amorphous ice and amorphous ice film (the thickness $D = 4$ nm) will be studied by using first principle molecular dynamics methods (FP-MD) with high precision in this paper. Since the simulation of T_g of nanoice with FP-MD is still difficult for too many atoms due to the limitation of computational power at present time, the classical MD method is, therefore, adopted as an auxiliary method for larger D. For comparison, the apparent glass transition temperature is also measured by analyzing the heat capacity of amorphous ice films with different film thicknesses as a function of temperature. In addition to important potential application in technological domain, such simulation may cast light onto the fundamental origins of the glass transition and improve our understanding of thermodynamic phase transitions for nanoscaled materials.

---

a)Author to whom correspondence should be addressed. Electronic mail: hecheng@mail.xjtu.edu.cn.

II. SIMULATION DETAILS

For amorphous ice bulk and films with the thickness $D = 4$ nm, simulations are performed using CASTEP software package based on density functional theory with the generalized gradient approximation of Perdew, Burke, and Ernzerhof exchange-correlation functionals.[16,17] Similar functions have been successfully used to study the structural and electronic properties of water.[18–20] In our work, the electron–ion interaction is described by ultrasoft pseudopotentials with a cutoff energy of 380 eV, where sufficient numbers of wave functions are included so as to get precise information about the electronic structure of the crystals. The density of the occupied states can be precisely described by supercells with 64 molecules for bulk amorphous ice and 128 molecules for 4 nm amorphous ice film.[21,22] We use Γ points to sample the 1D Brillouin zone during the dynamic simulation, and acquire HDA by pressurizing amorphous ice with hexagonal structure from the ambient pressure to pressure $P = 1.2$ GPa at 77 K (Ref. 4) and the simulation time is 30 ps. The simulated density ρ ($T = 77$ K, $P = 0.1$ MPa) of HDA equals 1.17 g/ml, which is in a good agreement with the experimental data.[4,22] On the other hand, LDA is formed by isobaric heating of HDA at 0.025 GPa and 137 K.[23] Subsequently, the LDA is decompressed and cooled down to 77 K. The obtained ρ ($T = 77$ K, $P = 0.1$ MPa) $= 0.92$ g/ml is corresponding to the experimental data of 0.94 g/ml.[24] In the simulation, the temperature is controlled by a Nosé–Hoover thermostat.[25]

To obtain T_g of LDA and the structure of supercooled water near T_g, simulation may be an ideal tool to realize the rapid heating while avoiding the crystallization of amorphous ice.[25] In the FP-MD methods, the heat capacity of bulk amorphous ice $C_{pb}(T)$ function plays an important role in understanding the thermodynamics of water. It is determined by[26]

$$C_{pb} = \frac{\partial H}{\partial T} = \frac{\langle \Delta H^2 \rangle}{kT^2}, \tag{1}$$

where k is Boltzmann's constant and $\langle \Delta H^2 \rangle$ is the mean-squared fluctuation in enthalpy.

Classical MD simulations are performed to simulate the amorphous ice bulk and films (the thickness $D > 4$ nm) in *NPT* statistical ensemble with the COMPASS (condensed-phase optimized molecular potentials for atomistic simulation studies) force field based on the earlier class II CFF9x and polymer-consistent force-field (PCFF) force fields, which is the first *ab initio* base force field and has been parameterized using extensive data for molecules in the condensed phase. P and T are kept constant, N is atom number, and T is imposed by the Nosé–Hoover algorithm.[27] The integration step is 1 fs using the Verlet-leap frog algorithm.[28] Configurations saved every 1 ps with a 2 K step per state at the range of 77 K $< T <$ 281 K are kept with 0.1 ns. The initial configuration for any given T is taken to be the final one from the previous T. When $t = 500$ ps, the error range is 1%, which is allowed in this simulation. This is also confirmed from our earlier simulation works and other literatures.[29–31] Therefore, in the later simulation, $t = 500$ ps is taken. After the MD simulation, fluctuations
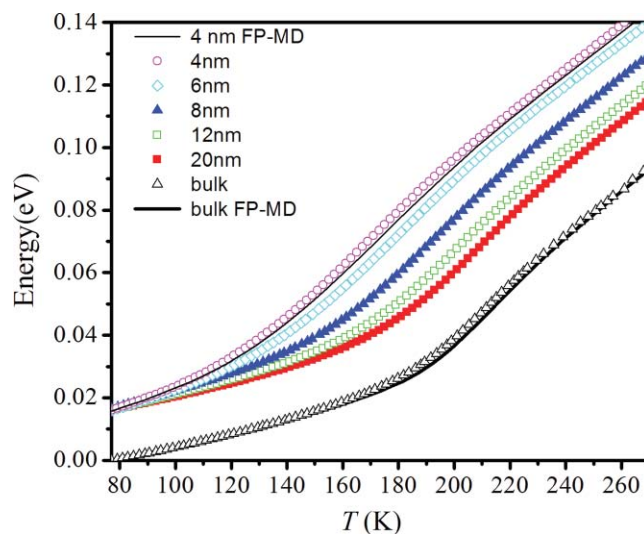

FIG. 1. The potential energy of amorphous ice film with different sizes. The symbols ◯ (the thickness = 4 nm), ◇ (the thickness = 6 nm), ▲ (the thickness = 8 nm), □ (the thickness = 12 nm), ■ (the thickness = 20 nm), and △ (the bulk amorphous ice film) show the MD simulation results. The lines show the FP-MD results of 4 nm and bulk amorphous ice film, respectively.

in *NPT* ensemble are analyzed. Thus, C_p at a given T can be calculated by

$$C_p(T) = \frac{1}{RT^2} \langle \delta(\kappa + p + PV)^2 \rangle, \tag{2}$$

where κ and p denote the instantaneous values of the kinetic and potential energy. P, V, and T show the familiar thermodynamic state variables. In addition, the notation δX means $X - \langle X \rangle$, where $\langle X \rangle$ denotes the equilibrium ensemble average value of quantity X. In the simulation, $\delta(\kappa + p + PV)^2$ is directly given by analyzing results.

III. RESULTS AND DISCUSSION

Figure 1 shows the potential energy of amorphous ice bulk and films ($D = 4$ nm) versus temperature using FP-MD, MD during heating processes. According to the bulk case, the variation exhibits three temperature regions. At the beginning, the potential energy has no distinct change, and the bulk amorphous ice shows an amorphous-state behavior. Upon heating, energy undergoes a relatively strong increase, and bulk amorphous ice undergoes a transition and exhibits a behavior intermediate between the amorphous and liquid states. Upon increasing the temperature, energy is relatively high compared to the case of the amorphous state. It can also be observed in Fig. 1 that the energy obtained by MD is a little higher than that obtained from FP-MD for both bulk amorphous ice and amorphous ice film ($D = 4$ nm). Although the FP-MD method is the best method to simulate T_g of amorphous ice films due to its high precision, it cannot be achieved when the thickness $D > 4$ nm for the limitation of computational power at present. So, we just simulate the potential energy of a 4 nm amorphous ice film by the FP-MD method and have compromised to choose the MD method to simulate the potential energy of amorphous ice film above 4 nm. Therefore, to explore T_g of amorphous ice films with
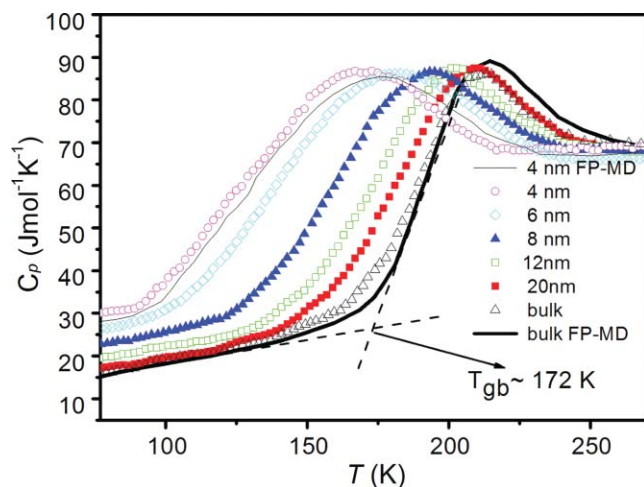
FIG. 2. The $C_{pb}(T)$ of amorphous ice film with different sizes. The symbols and lines have the same meanings with Fig. 1.

FIG. 3. The O–O RDFs of LDA at $D = 8$ nm as a function of T.

different thicknesses from 4 to 20 nm, we plot the potential energy versus heating temperature in Fig. 1 by the MD method. However, we can only get the rough regions rather than the exact value of T_g directly from Fig. 1. According to the definition of T_g, measuring the heat capacity $C_{pb}(T)$ is a direct way to obtain T_g.

Figure 2 plots $C_{pb}(T)$ of bulk amorphous ice and $C_p(T)$ of LDA with different thicknesses as a function of temperature, which are calculated by the temperature dependence of the total system energy with heating rate $q = 2 \times 10^{12}$ K s^{-1}. Following the usual experimental protocol, T_g is determined by the intersection of two slopes of the curves, as shown in Fig. 2. Therefore, $T_{gb\,(FP-MD)} = 171$ K, $\Delta C_{pb} \approx 43$ J mol^{-1} K^{-1} and $T_{gb\,(MD)} = 164$ K at $q = 2 \times 10^{12}$ K s^{-1} can be obtained. Extrapolation of the intrinsic $T_{gb\,(FP-MD)} = 164$ K and $T_{gb\,(MD)} = 159$ K at $q = 0.167$ K s^{-1} can be achieved according to Ref. 15. The theoretical predicted temperature of $T_{gb} = 165$ K at $q = 0.167$ K s^{-1} (Ref. 12) is only more than 1 K for FP-MD and about 6 K for MD method, respectively. According to the above results, FP-MD can be used to calculate the glass transition of bulk amorphous ice, and the difference between MD and FP-MD is about 4%. Meanwhile, we conclude that FP-MD method is more suitable to simulate the glass transition of bulk amorphous ice than MD method. The C_p (4 nm) versus T plot of amorphous ice films is also plotted in Fig. 2. $T_{g(FP-MD)}$ (4 nm) $= 97$ K and $T_{g\,(MD)}$ (4 nm) $= 93$ K. It is found that the T_g (4 nm) obtained by the FP-MD method is about 4% higher than that obtained by using the MD method, which corresponds to the result of bulk amorphous ice and is very useful for us to predict the corresponding FP-MD glass transition temperature. Therefore, the difference between MD and FP-MD is about 4%, which is suitable for both amorphous bulk ice and ice film. In the similar way, $T_{g(MD)}$ $(D) = 101, 127, 143,$ and 149 K when $D = 6, 8, 12,$ and 20 nm are also obtained according to Fig. 2. With the decreasing of thickness, the change of T_g exhibits the same trend, while the change of the energy exhibits opposite trend. The energy per atom of the amorphous ice film is higher than that of the bulk at the same temperature, which indicates the existence of the surface energy.
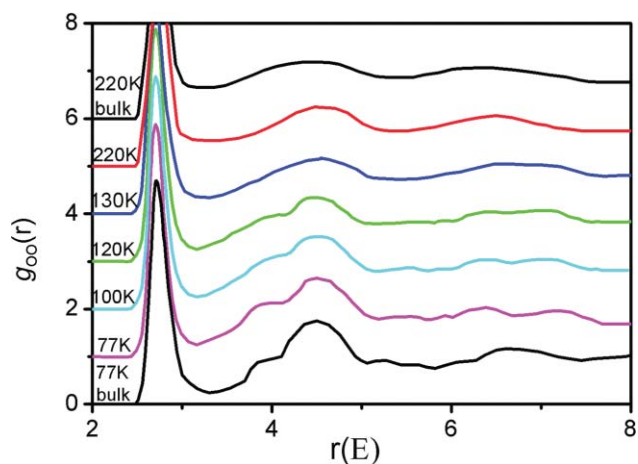
On the other hand, $T_g(D)$ can also be obtained with the O–O radial distribution functions (RDFs) of LDA as a function of T. We first choose the amorphous ice film with $D = 8$ nm to verify the results of our computational method. As shown in Fig. 3, at 130 K, the LDA shows a typical feature of a liquid structure. When $T < 130$ K, a remarkable splitting of the second peak of $g(r)$ is discernable whereas the third no longer appears, which prove the appearance of an amorphous structure.[32,33] Therefore, the $g(r)$ function of the system shows a clear glass transition in the temperature range of 120 K $< T <$ 130 K. The amorphous structure can be also seen in Fig. 4(a). However, when $T > 130$ K, the above amorphous structural characteristics disappear indicating the formation of liquid water. Meanwhile, the corresponding liquid structure is shown in Fig. 4(b).

To assist in the quantitative interpretation of these RDFs, near-neighbor coordination numbers N can be estimated from
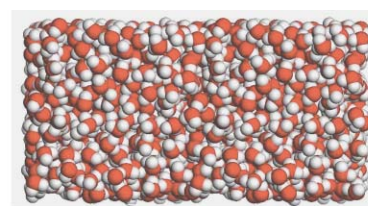
(a) **glass**
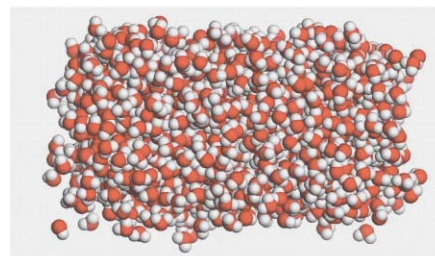
(b) **liquid**

FIG. 4. The sketch of 8 nm amorphous ice and liquid water film: (a) amorphous ice film and (b) liquid water film.

TABLE I. Coordination number of 8 nm amorphous ice film and bulk amorphous ice under different T conditions.

Structures	CN
$T = 77$ K bulk	3.98
$T = 77$ K 8 nm	3.65
$T = 100$ K 8 nm	3.67
$T = 120$ K 8 nm	3.68
$T = 130$ K 8 nm	3.84
$T = 300$ K 8 nm	3.89
$T = 300$ K bulk	4.30

these RDFs by integration[34]

$$N = 4\pi\rho \int_{r_{\min}}^{r_{\max}} r^2 g(r)\, dr, \tag{3}$$

where ρ is the number density of amorphous ice molecules and the integration range is normally chosen to coincide with minima in the respective RDFs.

The intermolecular coordination numbers give interesting insight into the nature of these differences. First, for the O–O data integrated between 2.3 and 3.3 Å, bulk LDA has 4.0 nearest neighbors at 77 K, that is consistent with the simulation result 3.9 (0.1) (Ref. 35) and within the errors, which is found in crystalline ice at 220 K, 3.7 (0.1). The liquid water value of 4.3 known from many studies is significantly greater than 4.0 and thus is slightly greater than the value of either LDA or crystalline ice Ih at 220 K. It is because that some molecules enter into the first neighbor shell from the second neighbor shell for the liquid liquidity. The CN of amorphous ice films with $D = 8$ nm versus temperature are also shown in Table I, which is apparently less than the value of bulk amorphous ice. Too many atoms on the surface make the CN decrease as the increase of surface/volume ratio. The value of CN increases obviously between 120 and 130 K for the liquid. It is also an actual evidence to prove T_g (8 nm) is between 120 and 130 K, which is a good agreement with the results obtained in Fig. 2.

Partial density of state (PDOS) provides information of the atoms, which influences the electronic state through variation in the angular momentum of the states. The PDOS can be obtained by analyzing the simulated structure. The PDOS exhibits integral intensities of different bands. The valence state of O can be attained by determining the distribution of O-2p electrons in t_{2g} and e_g^b bands. In this case, t_{2g} denotes the bands from -2.5 to 0.9 eV, which point away from H and form nonbonding bands. Here, e_g^b represents the bonding bands from -8 to -2.5 eV, which are occupied by the p_x, p_y, and p_z orbitals to overlap with the s orbital of H along the tetrahedron directions. The rest bands are the antibonding bands e_g^*, which consist of the states from 4 to 7 eV with the electrons polarized by the lone pair nonbonding states.[36]

The PDOS of amorphous ice film ($D = 4$ nm) at different temperatures by FP-MD methods are shown in Fig. 5 and the integral intensity values $N(\varepsilon)$ of O-2p are listed in Table II. The PDOS near Fermi level is mainly dominated by p electrons of the O atom and a part of the s electrons of the H atom. The fully occupied sets of bands with higher energy
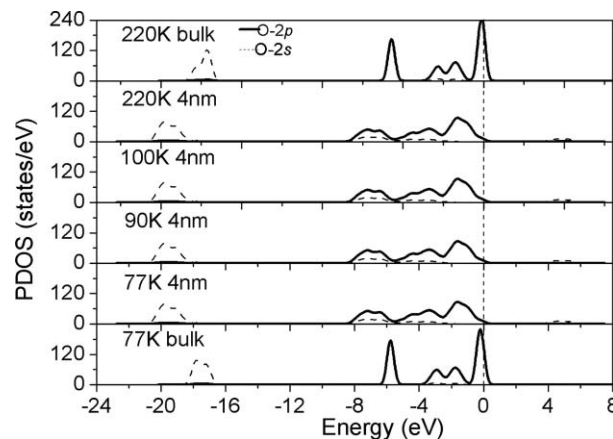

FIG. 5. PDOS of 4 nm amorphous ice film at different temperatures. $E_f = 0$ (vertical dotted line) is taken.

level consist of the overlapping bands of both O-2p and H-1s states indicating a strong interaction between the two states.

As shown in Table II because the four hydrogen bonds (H-bonds) structure of LDA are almost independent of the temperature range of 77 K $\leq T \leq$ 90 K, the variation of $N(\varepsilon) - e_g^b$ is limited. When $T = 100$ K, $N(\varepsilon)$-e_g^b is 3.22 lower than that at 90 K. The contribution of $2p$ electrons in $2p$–$1s$ hybridization of O–H becomes weaker as T increases. This implies that the equilibrium of four H-bonds structure in LDA is broken and the structure has a smaller number of H-bonds than LDA, showing that it is liquid.

In this work, the geometric definition is employed in order to quantify the number of hydrogen bonds in the amorphous ice. The hydrogen bond is defined by the following criteria: (1) the distance between hydrogen atom and acceptor is ≤ 2.5 Å and (2) a hydrogen atom is located between two oxygen ions, such as $\angle$OHO $> 140°$. This definition is within the trends of the simulation conditions in the other works.[34] Based on this definition, in the amorphous ice film ($D = 4$ nm), some one or two hydrogen-bonded amorphous ice molecules are found at 77 K where there are 3.92 hydrogen bonds (average) per amorphous ice molecule for the effect of surface molecules. When amorphous ice is heated to 90, 100, and 110 K, the number decreases to 3.90, 3.79, and 3.78, respectively. When it becomes liquid, some four hydrogen-bonded amorphous ice molecules turn into triply hydrogen-bonded structure.[7] Therefore, there is a distinct decrease between 90 and 100 K, which is also a glass transition

TABLE II. Integrated intensities of O-2p bands $N(\varepsilon)$-e_g^*, $N(\varepsilon)$-t_{2g}, and $N(\varepsilon)$-e_g^b in 4 nm amorphous ice film and bulk amorphous ice under different T conditions.

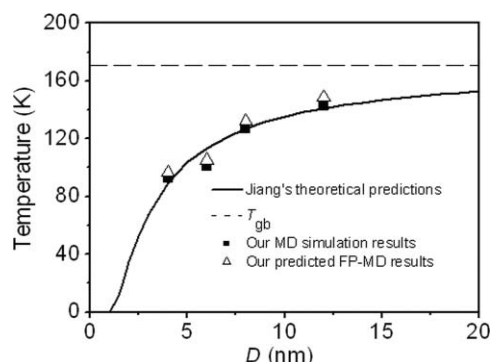| Structures	$N(\varepsilon)$-e_g^*	$N(\varepsilon)$-t_{2g}	$N(\varepsilon)$-e_g^b	Total
$T = 77$ K bulk	1.74	130.86	204.82	337.42
$T = 77$ K 4 nm	1.27	136.32	198.12	335.71
$T = 90$ K 4 nm	1.28	136.42	198.04	335.74
$T = 100$ K 4 nm	1.26	140.04	194.82	336.12
$T = 300$ K 4 nm	1.29	142.04	191.89	335.93
$T = 300$ K bulk	1.76	140.61	196.00	338.37

FIG. 6. A comparison $T_g(D)$ of amorphous ice films between the model predictions (solid line) and the simulation MD results (the symbols ■). The symbols △ show our predicted FP-MD results according to the difference between MD and FP-MD. The dashed line shows the glass transition temperature of bulk amorphous ice film. The necessary parameters are $h = 0.318$ nm,[40] and $\Delta C_{pb} \approx 43$ J mol^{-1} K^{-1}.

behavior. The results are corresponded with the analysis of heat capacity, RDFs, and the electronic structure.

A theoretical model is also compared with our simulation results. The size-dependent glass transition temperature function $T_g(D)$ of films is given by[37]

$$T_g(D)/T_{gb} = \exp[2\Delta C_{pb}/(3R)/(1 - D/2h)], \quad (4)$$

where T_{gb} is the glass transition temperature for the corresponding bulk value of $T_g(D)$, D denotes the thickness, R is the ideal gas constant, and h is the atomic diameter.[38,39] Here, ΔC_{pb} is the heat capacity difference between the bulk glass and the bulk liquid at T_{gb} and is positive.

According to Eq. (4), T_g of amorphous ice films can be quantitatively determined without the free parameter, which is shown in Fig. 6. For convenient comparison, our MD simulation results (solid symbols), and the corresponding FP-MD results, which are predicted (open symbols) by the difference 4% between MD and FP-MD methods, are also shown in Fig. 6. It is shown that the glass transition temperature decreases with the decreasing thickness of amorphous ice film, and the variation tendency of the results is consistent with the simulation results in the size range. The agreement shown in Fig. 6 indicates that the MD method is suitable to simulate the potential energy with different thicknesses and $C_p(T, D)$ plots, but it needs to be modified to corresponding FP-MD results. As shown above, $T_g(D)$ function for amorphous ice film can be satisfactorily described as long as the related thermodynamic parameters are already known.[41] Our MD simulation and predicted FP-MD T_g of amorphous ice films are good corresponding to the theoretical models.

IV. CONCLUSIONS

In summary, the glass transition behaviors of amorphous ice films with different thicknesses have been characterized by a pronounced $C_p(T, D)$ peak with different simulation methods. The $g(r)$ function and CN of 8 nm amorphous ice film show a clear glass transition in the temperature range of 120 K $< T <$ 130 K by MD method.

And integral intensities of PDOS and hydrogen-bonded structure of 4 nm amorphous ice film show the glass transition temperature in the range of 90 K $< T <$ 100 K by FP-MD method. Hence, the glass transition temperature with different thicknesses is confirmed by analyzing hydrogen-bond network, the RDFs, and relationship between H-bonds and electronic structures. Comparing with other methods, the FP-MD has added flexibility to the standard implementations and has made it possible to study dynamical processes, such as structural transformations of covalently bonded materials as well as chemical reactions in the process of glass transition. However, the evident problem of FP-MD is the large computational capacity at present. Meanwhile, our simulation results of amorphous ice films are in accordance with the theoretical $T_g(D)$ function.

[1] H. E. Stanley, S. V. Buldyrev, M. Canpolat, M. Meyer, O. Mishima, M. R. Sadr-Lahijany, A. Scala, and F. W. Starr, Physica A **257**, 213 (1998).
[2] P. Ehrenfreund, H. J. Fraser, J. Blum, J. H. E. Cartwright, J. M. García-Ruiz, E. Hadamcik, A. C. Levasseur-Regourd, S. Price, F. Prodi, and A. Sarkissian, Planet. Space Sci. **51**, 473 (2003).
[3] P. Jenniskens, D. F. Blake, M. A. Wilson, and A. Pohorille, Astrophys. J. **455**, 389 (1995).
[4] V. Velikov, S. Borick, and C. A. Angell, Science **294**, 2335 (2001).
[5] C. A. Angell, Science **319**, 582 (2008).
[6] E. Mayer, J. Appl. Phys. **58**, 663 (1985).
[7] Y. P. Handa and D. D. Klug, J. Phys. Chem. **92**, 3323 (1988).
[8] G. P. Johari, A. Hallbrucker, and E. Mayer, Nature **330**, 552 (1987).
[9] A. Hallbrucker, E. Mayer, and G. P. Johari, J. Phys. Chem. **93**, 7751 (1989).
[10] K. Ito, C. T. Moynihan, and C. A. Angell, Nature **398**, 492 (1999).
[11] G. P. Johari, J. Chem. Phys. **116**, 8067 (2002).
[12] Y. Z. Yue and C. A. Angell, Nature **427**, 717 (2004).
[13] M. Alcoutlabi and G. B. McKenna, J. Phys.: Condens. Matter **17**, R461 (2005).
[14] C. He, J. S. Lian, and Q. Jiang, J. Phys. Chem. B **111**, 11177 (2007).
[15] Y. Z. Yue, J. Non-Cryst. Solids **354**, 1112 (2008).
[16] D. P. Segall, J. D. Linadan, M. J. Probert, C. J. Pickard, P. J. Hasnip, S. J. Clark, and M. C. Payne, J. Phys.: Condens. Matter **11**, 2717 (2002).
[17] J. P. Perdew, K. Burke, and M. Ernzerhof, Phys. Rev. Lett. **77**, 3865 (1996).
[18] E. Schwegler, G. Galli, F. Gygi, and R. Q. Hood, Phys. Rev. Lett. **87**, 265501 (2001).
[19] P. H. Hahn, W. G. Schmidt, K. Seino, M. Preuss, F. Bechstedt, and J. Bernholc, Phys. Rev. Lett. **94**, 037404 (2005).
[20] S. W. Wang, Y. Z. Cao, and P. A. Rikvold, Phys. Rev. B **70**, 205410 (2004).
[21] D. Prendergast, J. C. Grossman, and G. J. Galli, Chem. Phys. **23**, 014501 (2005).
[22] J. L. Kuo and W. F. Kuhs, J. Phys. Chem. B **110**, 3697 (2006).
[23] C. He, J. S. Lian, and Q. Jiang, Chem. Phys. Lett. **437**, 45 (2007).
[24] M. E. Tuckerman, Y. Liu, G. Ciccotti, and G. J. Martyna, J. Chem. Phys. **115**, 678 (2001).
[25] E. G. Ponyatovsky, V. V. Sinitsyn, and T. A. Pozdnyakova, J. Chem. Phys. **109**, 2413 (1998).
[26] K. A. Sharp and B. Madan, J. Phys. Chem. B **101**, 4343 (1997).
[27] S. Nose, J. Chem. Phys. **81**, 511 (1984).
[28] J. M. Haile, Molecular Dynamics Simulation (Wiley, New York, 1992).
[29] Z. M. Ao and Q. Jiang, Langmuir **22**, 1241 (2006).
[30] N. C. Karayiannis, V. G. Mavrantzans, and D. N. Theodorou, Macromolecules **37**, 2978 (2004).

[31] A. Soldera, Polymer **43**, 4269 (2002).

[32] B. Francesca and F. Riccardo, Rev. Mod. Phys. **77**, 371 (2005).

[33] Y. Chen, X. F. Bian, J. X. Zhang, Y. N. Zhang, and L. Wang, Modelling Simul. Mater. Sci. Eng. **12**, 373 (2004).

[34] Y. Waseda, The Structure of Non-Crystalline Materials (McGraw-Hill, New York, 1980).

[35] J. L. Finney, A. Hallbrucker, I. Kohl, A. K. Soper, and D. T. Bowron, Phys. Rev. Lett. **88**, 225503 (2002).

[36] C. Q. Sun, Prog. Mater. Sci. **48**, 521 (2003).

[37] Q. Jiang, H. X. Shi, and M. Zhao, J. Chem. Phys. **111**, 2176 (1999).

[38] Q. Jiang, H. X. Shi, and J. C. Li, Thin Solid Films **354**, 283 (1999).

[39] Y. F. Zhu, J. S. Lian, and Q. Jiang, J. Phys. Chem. C **113**, 16896 (2009).

[40] W. X. Zhang, C. He, J. S. Lian, and Q. Jiang, Chem. Phys. Lett. **421**, 251 (2006).

[41] M. Wautelet, J. Phys. D: Appl. Phys. **24**, 343 (1991).